Available online at www.sciencedirect.com
ScienceDirect
Journal of Computational Physics 226 (2007) 2133–2145
JOURNAL OF COMPUTATIONAL PHYSICS
www.elsevier.com/locate/jcp

Test particle method for incorporation of the kinetic effects into the envelope simulations of Raman backscattering

Min Sup Hur, Hyyong Suk *

Center for Advanced Accelerators, Korea Electrotechnology Research Institute, KERI, 28-1 Seongju-dong, Changwon-city, Kyungnam 641-120, Republic of Korea

Received 11 October 2006; received in revised form 19 June 2007; accepted 28 June 2007
Available online 21 July 2007

Abstract

A new test particle method is presented for self-consistent incorporation of the kinetic effects into the fluid three-wave model. One of the most important kinetic effects is the electron trapping and it has been found that the trapping affects significantly the behavior of Raman backscatter and Raman backward laser amplification. The conventional fluid three-wave model cannot reproduce the kinetic simulations in the trapping regime. The test particle scheme utilizes the same equations for the laser evolution as in the three-wave model. However, the plasma wave is treated by the envelope-kinetic equation, which consists of envelope evolution and the kinetic term. The core of the new scheme is employing test particles to compute the kinetic term self-consistently. The benchmarking results against the averaged particle-in-cell (aPIC) code show excellent agreements, and the computation speed gain over the aPIC is from 2 to 20 depending on parameters.

PACS: 42.65.Dr; 52.38.−r; 52.65.−y

Keywords: Kinetic effect; Test particle; Raman backscatter; Plasma; Laser

1. Introduction

The laser-plasma systems such as laser wakefield accelerator (LWFA), Raman backward amplification (RBA) of laser pulses in a plasma, and inertial fusion systems are considerably affected by the kinetic effects of the plasma. Among numerous kinetic effects, the particle trapping by the wavebreaking is studied intensively because it has been found to dominate the behavior of the laser-plasma systems. For instance, an electron beam can be self-injected by the particle trapping mechanism in the laser wakefield accelerators [1,2]. For the case of Raman backscattering (RBS), there have been a series of intensive studies of the trapped particle effects on the amplification efficiency of RBA [3–5] and Raman reflectivity in the inertial fusion plasmas [6,7].

* Corresponding author. Tel.: +82 55 280 1451; fax: +82 55 280 1469.
E-mail address: hysuk@keri.re.kr (H. Suk).

0021-9991/$ - see front matter © 2007 Elsevier Inc. All rights reserved.
doi:10.1016/j.jcp.2007.06.032

In many cases, the particle trapping is induced by the wavebreaking of a plasma wave. Since the wavebreaking means mathematically the disappearance of a single valued solution of the fluid equation [8], it is impossible to model the trapping process with unmodified fluid equations of the plasma. Instead of the fluid model, the particle-in-cell (PIC) method has been widely used to self-consistently reflect the wavebreaking and other kinetic effects in RBA [4,9,10] and LWFA [11,12]. The importance of kinetic simulations can be seen easily in Refs. [4,9], where for the Raman backward amplifier, the full kinetic simulations show quite different results from the conventional fluid three-wave calculation in the trapping-dominant regime. However, it is becoming a more and more challenging task to simulate large scale laser-plasma systems by PIC due to its extremely slow computation speed. In an effort to reduce the computational cost while keeping the high accuracy of PIC, several reduced models have been invented: the reduced PIC (rpic) [13] for the simulations of the decay instabilities including RBS, and quickPIC [14] and turbowave [15] for LWFA. For RBS and RBA simulations the averaged-PIC (aPIC) [16] code was developed and it was successful in reproducing the full PIC results in the highly kinetic regime [4]. In the averaged-PIC model, the lasers are treated by envelope equations, which enable the averaging-out of the fast spatio-temporal scales, while the plasma is solved fully kinetically by the conventional PIC technique. The advantage of such hybrid combinations is that the simulation time step can be fit to the slowly varying plasma rather than the fast-oscillating lasers. The resultant gain in the computation speed becomes ω/ω_p, where ω_p and ω represent the plasma and laser frequencies, respectively and typically $\omega \gg \omega_p$.

The change from the full PIC to the averaged-PIC (or other similar codes) is conceptually a reduction from field–particle interaction into envelope–particle interaction. For RBA simulations, it was found that the averaged-PIC model can be reduced even more into what is called the test particle method, which is the major subject of this paper. In the second reduction, i.e. the test particle scheme, the basic equations are almost the same as in the conventional three-wave fluid model. However, the most distinctive feature of the new method is the envelope-kinetic equation of the plasma wave [3,5], where a kinetic term is added to the fluid-based envelope equation of the plasma wave. The kinetic term is represented by an ensemble average of $v^2/c^2\exp(-i\phi)$, where v is the particle velocity and ϕ the ponderomotive phase of the particle. To calculate self-consistently the contribution of the trapped particles to the ensemble average, some test particles are employed and their motions are kept track of. The remaining bulk plasma contribution to the kinetic term is obtained from the linear theory and proper approximations. The test particles do not generate any electric field. Instead, the electric field is reconstructed from the plasma wave envelope, which is obtained from the envelope-kinetic plasma equation. The role of simulation particles is not the generation of field and current, but giving ensemble averaged kinetic effects. Therefore, the test particle scheme is a reduction from the envelope–particle interaction of the aPIC into the envelope–envelope interaction, while important kinetic effects are self-consistently counted via the test particle calculation of the kinetic term.

The test particle scheme has advantages in the computation speed and in treating the thermal noise. From the notion that the kinetic effects are determined dominantly by trapped particles, the code takes only some fraction of the whole plasma, which are to be involved in the trapping process. Those particles are typically located at the high-velocity region in the velocity space. Considering the fact that tracing the motion of huge number of simulation particles in full or reduced type PICs is the most time-consuming part, decreasing the number of particles is a dominant factor in the computation speed gain. The other advantage is related with the sensitivy of RBS to the thermal noise of the plasma. A single simulation particle (often called 'superparticle') corresponds to a huge number of real particles, which enhances numerically the thermal noise. Such an enhanced noise often leads to an overestimated pump depletion in RBS process. The test particle scheme is free from such an issue, since the thermal fluctuation of the plasma is smoothed out.

In this paper, we present the details of the test particle scheme, applying it to the Raman backscatter and Raman backward laser amplifier. The latter, briefly RBA, has been attracting much interest recently due to its possibility to obtain more than a peta-watt level, ultra-short laser pulse in a compact device using plasmas. In this system, the trapped particles were found to deteriorate the amplification efficiency [3,5] by the suppressed RBS. The mechanism of RBS suppression should be fully understood and its negative effects must be eventually surmounted to reach the original goal. For the intensive kinetic studies of the system, a fast and higly accurate kinetic simulation code is very important, and the test particle method is believed to be a good candidate for that.

The rest of this paper is organized as follows. In Section 2 the conventional fluid three-wave model, the averaged-PIC equations, and the envelope-kinetic equation for the plasma wave are summarized. In Section 3, the details of the test particle algorithm is provided. The benchmarking results of the new code against the aPIC simulations are also presented in Section 3. Finally the paper is summarized in Section 4.

2. Laser amplification using RBS in plasmas

The system of Raman backward amplification (RBA) is composed of a plasma and two counter-propagating lasers. One of the lasers is a seed, which is typically a weak and short pulse. The other laser is the pump, which is the energy source for the amplification. Its intensity is much stronger compared to the seed and the pulse duration in the longitudinal direction is large. The pump frequency is slightly higher than the seed frequency, where the difference is almost the same as the plasma frequency. When those two pulses collide inside the plasma, the ponderomotive force by the beat of the lasers resonantly drives the plasma wave. The density fluctuation of the plasma induced in this way scatters backward (Raman backscattering, RBS) the high frequency pump laser. Because in RBS the frequency is downshifted by the plasma wave frequency, the backscattered pump correlates with the counter-coming seed laser. Thus the seed gets the pump energy by RBS process. This energy transfer occurs with an instability mechanism: the amplified seed excites the plasma wave more strongly, and the enhanced plasma fluctuation scatters the pump laser more efficiently, which eventually increases the energy transfer rate.

There are several different models to describe RBA. In this section, we summarize the conventional fluid three-wave model, the averaged-PIC, and the envelope-kinetic equation of the plasma wave. The general PIC scheme is already well known, so its algorithm is not addressed here.

2.1. Fluid three-wave equations

When the idea of laser amplification using RBS was proposed [17], a set of the one-dimensional three-wave equations was the basic model of the system. To derive the three-wave model the laser and plasma wave field are decomposed into their slowly varying envelopes and fast oscillation terms

$$A_{\text{Laser}}(z,t) = 0.5(\widetilde{A}_1 \mathrm{e}^{\mathrm{i}k_1 z - \mathrm{i}\omega_1 t} + \widetilde{A}_2 \mathrm{e}^{-\mathrm{i}k_2 z - \mathrm{i}\omega_2 t}) + \text{c.c.}, \tag{1}$$

and

$$E_z(z,t) = 0.5\widetilde{E}_z \mathrm{e}^{\mathrm{i}\Delta k z - \mathrm{i}\Delta\omega t} + \text{c.c.}, \tag{2}$$

where A_{Laser} is the magnetic vector potential of the lasers, $\widetilde{A}_{1,2}$ represent the slowly varying parts (envelopes) of the seed and pump lasers, respectively, $k_{1,2}$ and $\omega_{1,2}$ the wavenumbers and frequencies of the lasers, and $\widetilde{E}_z$ the plasma wave envelope. Note that the minus sign in front of k_2 indicates that pump laser propagates to the left direction. Note also that the phase in the eikonal part of the plasma wave is defined by $\Delta k z - \Delta\omega t = (-k_2 - k_1)z - (\omega_2 - \omega_1)t$, since the plasma wave is driven by the beat of the two lasers. Next step is replacing the decomposed field into the wave equation

$$-\frac{\partial^2 \vec{A}_{\text{Laser}}}{\partial z^2} + \frac{1}{c^2}\frac{\partial^2 \vec{A}_{\text{Laser}}}{\partial t^2} = \mu_0 \vec{J} + \frac{\partial \vec{E}_z}{\partial t} \tag{3}$$

and the momentum equation of the plasma

$$\frac{\partial \vec{v}}{\partial t} + \vec{v}\cdot\nabla\vec{v} = -\frac{e}{m}(\vec{E} + \vec{v}\times\vec{B}), \tag{4}$$

where $\vec{J}$ is the electron current, $\vec{v}$ the fluid velocity of the electron, $\vec{E}$ the electric field of the lasers and plasma wave, $\vec{B}$ the magnetic field of the laser defined by $\vec{B} = \nabla \times \vec{A}_{\text{Laser}}$. Combining Eqs. (1)–(4) and averaging out the spatio-temporally fast eikonal terms, yields the following envelope equations of the lasers and plasma wave

$$\frac{\partial a_1}{\partial t} + c\frac{\partial a_1}{\partial z} = -\frac{\omega_p(\omega_1+\omega_2)}{4\omega_1}a_2 f^*, \quad \frac{\partial a_2}{\partial t} - c\frac{\partial a_2}{\partial z} = \frac{\omega_p(\omega_1+\omega_2)}{4\omega_2}a_1 f, \tag{5}$$

and

$$\frac{\partial f}{\partial t} + i\delta\omega f = -\frac{\omega_1+\omega_2}{4}a_1^* a_2, \tag{6}$$

where $a_{1,2}$ are the normalized envelopes of the lasers, f the normalized plasma wave envelope, and ω_p the plasma frequency. The normalizations are defined by $a_{1,2} = e\widetilde{A}_{1,2}/mc^2$ and $f = e\widetilde{E}_z/mc\omega_p$. The second term in the left-hand-side (LHS) of Eq. (6) is the detuning between the plasma frequency and the ponderomotive driving frequency, defined by $\delta\omega = \omega_p - (\omega_2 - \omega_1)$.

2.2. Averaged-PIC model

As the fluid-based three-wave equations do not predict well the amplification in the kinetic regime, the simulation studies by PIC codes have been performed [9,17] in parallel to the analytic works. Though the PIC method is self-consistent in describing every kinetic effect, the slow computation time is an obstacle to the intensive and systematic study of RBA. As a reduced model, the envelope-kinetic equations for lasers, which are commonly used in free-electron-laser (FEL) study in similar forms, were employed by Shvets et al. [18,19]

$$\frac{\partial a_1}{\partial t} + c\frac{\partial a_1}{\partial z} = -\frac{i\omega_p^2}{2\omega_1}a_2\langle e^{+i\phi_j}\rangle, \quad \frac{\partial a_2}{\partial t} - c\frac{\partial a_2}{\partial z} = -\frac{i\omega_p^2}{2\omega_2}a_1\langle e^{-i\phi_j}\rangle, \tag{7}$$

where $\phi_j = -(k_1+k_2)z_j - (\omega_2-\omega_1)t$ is the ponderomotive phase of the jth particle, and $\langle\rangle$ the ensemble average of simulation particles in ponderomotive buckets. In averaged-PIC code [16], these equations are used for laser evolution and the plasma is treated by the conventional PIC method. Because the simulation time step is determined in terms of the relatively slow plasma time scale, overall calculation speed of aPIC increases from a full PIC code by a factor of ω/ω_p. The benchmarking of the aPIC against a full PIC can be found in Refs. [4,16].

2.3. Envelope-kinetic equation of plasma wave

Comparison of Eq. (5) to Eq. (7) leads to the definition of a scaled bunching parameter F

$$F \equiv -i\frac{\omega_p}{\omega}\langle e^{-i\phi_j}\rangle, \tag{8}$$

where $\omega = (\omega_1+\omega_2)/2$. By this definition the envelope-kinetic laser equations take exactly the same form as the laser envelope equations with f replaced by F. Then it is expected that the parameter F should follow a similar equation as Eq. (6). The equation of F can be derived starting from the first and second time derivative of F

$$\frac{\partial F}{\partial t} = i\Delta\omega F + c(k_1+k_2)\frac{\omega_p}{\omega}\langle\beta_j e^{-i\phi_j}\rangle, \tag{9a}$$

$$\frac{\partial^2 F}{\partial t^2} = i\Delta\omega\frac{\partial F}{\partial t} + i\Delta\omega c(k_1+k_2)\frac{\omega_p}{\omega}\langle\beta_j e^{-i\phi_j}\rangle + ic^2(k_1+k_2)^2\frac{\omega_p}{\omega}\langle\beta_j^2 e^{-i\phi_j}\rangle + c(k_1+k_2)\frac{\omega_p}{\omega}\left\langle\frac{\partial\beta_j}{\partial t}e^{-i\phi_j}\right\rangle, \tag{9b}$$

where $\beta_j = v_j/c$ is the velocity of the jth particle normalized to the speed of light. Eliminating $\langle\beta_j e^{-i\phi_j}\rangle$ from Eqs. (9a) and (9b), and replacing $\partial_t\beta_j$ term by the equation of a single particle motion yields the envelope-kinetic equation of F

$$\frac{\partial F}{\partial t} + i\delta\omega F + 2\omega\langle\beta_j^2 e^{-i\phi_j}\rangle = -\frac{\omega}{2}a_1^* a_2. \tag{10}$$

Note that many unimportant high harmonics and slowly varying terms were dropped in Eq. (10), of which the details can be found in Refs. [3,5]. Eq. (10) is the same as Eq. (6) except $2\omega\langle\beta_j^2 e^{-i\phi_j}\rangle$ in the LHS, which is called the kinetic term.

3. Test particle simulation of RBA

In this section, we describe the details of the test particle algorithm for simulations of Raman backscattering (RBS) and Raman backward amplification (RBA) of a laser pulse in a plasma. The benchmarking results of the new simulations against the aPIC are also presented.

The core elements composing the test particle method are the laser envelope solver, the envelope-kinetic equation solver, the test particles to calculate the kinetic term in Eq. (10), and the test particle loader. Other than those core parts, there are accessorial routines such as moving window shifter, input/output interface, and various diagnostic routines. The test particle code employs the explicit scheme in upgrading the field and particle data. The structure of the code and the explicit data flow are shown in Fig. 1. In the following sections we describe the detail of each routine.

3.1. Test particle loading

The kinetic effects are determined dominantly by the trapped particles. Thus, in the test particle scheme, they do not need to load all particles in the velocity distribution, but it is enough to use ones, which are to be trapped during the simulation. Since the trapping occurs when a particle velocity exceeds the phase velocity of the plasma wave, the test particle code loads the particles located initially near the phase velocity, u_ϕ (see Fig. 2).

For all the simulations presented in this paper, we used the left half of the initial Gaussian distribution as test particles. More exactly speaking, the velocity range of the test particles goes from -3σ through 0, where the Gaussian distribution is defined by $f(u) = \pi\exp(-u^2/\sigma^2)/\sigma$. It was shown in the previous work [3] that the fraction of the trapped particles near the peak of the seed is just a few percent. However, the test particle portion goes up to several tens of percent in the tail of the amplified seed. Though the rear part behind the tail is

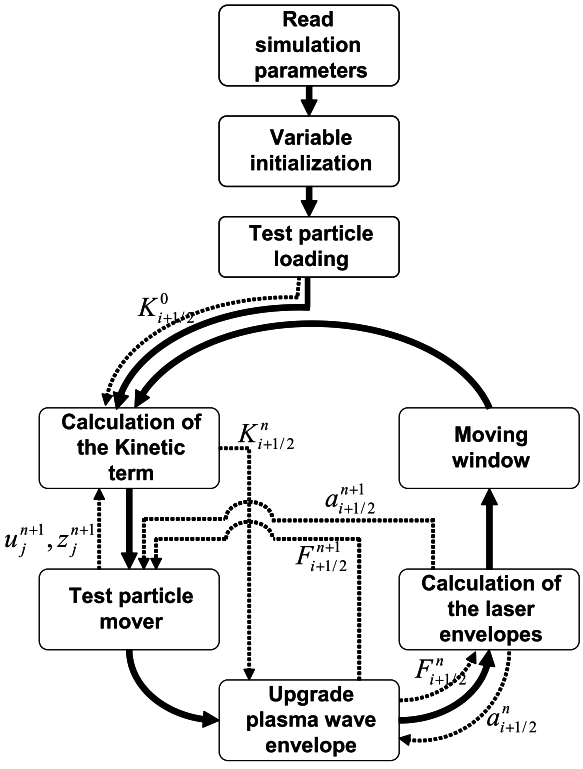

Fig. 1. Structure of the test particle code. The solid arrows represent the sequence of routines and the dotted arrows are the data flow.

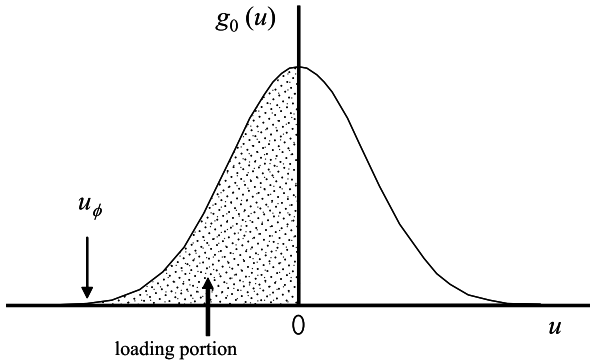

Fig. 2. Loading portion of the test particles in the velocity distribution.

not physically important, the velocity range of the test particles should be large enough to keep the self-consistency in the whole domain of the simulation.

It should be noted that using a half of the simulation particles in the new scheme does not mean that the calculation speed-up is just a factor of two. Since the basic field solvers in the test particle code are from the envelope equations, the numerical thermal noise is much less important in the test particle scheme than in other general PICs including the aPIC. Thus the absolute number of simulation particles can be much smaller in the test particle scheme, which enhances even more the computation speed gain. The details are discussed in Section 3.5.

3.2. Simulation mesh and calculation of the kinetic term

The envelopes of laser and plasma wave and the kinetic term are computed at the center of the mesh as in Fig. 3. Because the fast spatial oscillation terms have been averaged out, the mesh size can be just large enough to resolve the slowly varying envelopes. In our simulations, the mesh size was set to be the same as the beat wavelength of two counter-propagating lasers, which is almost half of the laser wavelength, so

$$\Delta z = \frac{2\pi}{k_1 + k_2} = \frac{\lambda_1 \lambda_2}{\lambda_1 + \lambda_2}. \tag{11}$$

The $(i + 1/2)$th kinetic term, $K_{i+1/2}$ is obtained from the ensemble average of the test particles located between the i and $(i + 1)$th grids. Since the test particle code does not load the full particle distribution, there should be some manipulation of the kinetic term to approximate its value from the incomplete particle informations. The first process is the separation of the kinetic term into the contributions by trapped and untrapped particles, i.e.

$$2\omega\langle\beta_j^2 e^{-i\phi_j}\rangle = 2\omega\langle\beta_{j,\mathrm{trap}}^2 e^{-i\phi_j}\rangle + 2\omega\langle\beta_{j,\mathrm{untrap}}^2 e^{-i\phi_j}\rangle \equiv K_t + K_u. \tag{12}$$

Because the velocity range of the test particles (one-half of the distribution) is large enough to cover all the trapping, it is possible to calculate K_t directly from the simulation particles without approximation. An impor-

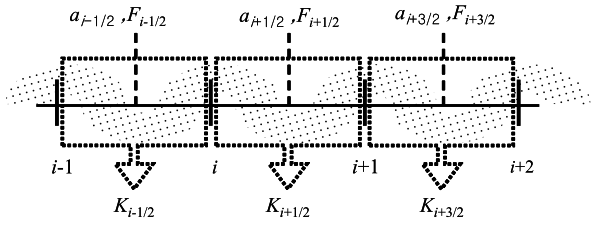

Fig. 3. The mesh structure of the test particle code.

tant point in this procedure is grouping the particles into the 'trapped' and 'untrapped'. The criterion of such classification is the phase velocity of the plasma wave $u_\phi = (\omega_1 - \omega_2)/(k_1 + k_2)$. Every time step the velocities of all the particles are compared to u_ϕ. Once the velocity (u) of a particle is found to be more negative than u_ϕ, i.e. $|u| > |u_\phi|$, it remains 'trapped' until the simulation ends. Only such trapped particles are counted in computing K_t.

The other part of the kinetic term K_u requires some approximation since the particle distribution is not complete. A linear analysis of the kinetic term [5] is used for this procedure. The kinetic term can be represented by an integral form [5] as

$$2\omega\langle\beta_j^2 e^{-i\phi_j}\rangle = 2\omega\int_\lambda dz\int_{-\infty}^{\infty} g(\beta)\beta^2 e^{-i\phi}\,d\beta, \tag{13}$$

where $g(\beta)$ is the velocity distribution function. From the linearization of the Vlasov equation (13) can be represented by

$$2\omega\langle\beta_j^2 e^{-i\phi_j}\rangle \simeq i\omega\omega_p F_1\int_{-\infty}^{\infty}\frac{\beta^2\partial_\beta g_0}{\Delta\omega + 2\omega\beta}\,d\beta, \tag{14}$$

where g_0 is the initial velocity distribution. Note that in Eq. (14) we neglected the real part, which is responsible for the linear Landau damping, since it is very small in the temperature range considered here. In the nontrapping regime, the zero'th order distribution $g_0(\beta)$ covers the velocity range from $-\infty$ to ∞ (in the actual simulation, the distribution is cut off at $\pm 3\sigma$). In this regime the integration in Eq. (14) results in the well-known thermal shift of the Langmuir wave frequency [5].

$$2\omega\langle\beta_j^2 e^{-i\phi_j}\rangle = iF_1\frac{3k_b^2 T_e}{2\omega_p^2 m}, \tag{15}$$

where T_e is the electron temperature and m the electron mass. However, in the trapping regime, K_u counts only the 'untrapped' particles, and the integration range in Eq. (14) should be changed, since some particles have been depleted from the initial g_0 by the trapping (see Fig. 4).

$$K_u = 2\omega\langle\beta_{j,\mathrm{untrap}}^2 e^{-i\phi_j}\rangle \simeq i\omega\omega_p F_1\int_{\hat\beta}^{\infty}\frac{\beta^2\partial_\beta g_0}{\Delta\omega + 2\omega\beta}\,d\beta, \tag{16}$$

where the upper limit is replaced by 3σ in the actual computation. To find the lower limit $\hat\beta$, the code checks the number of trapped particles n_t every time step. If the number of simulation particles in the whole zeroth distribution g_0 is defined by N_0 (note that the number of test particles is then $N_0/2$), $\hat\beta$ can be found by numerically inverting the following integration

$$\frac{n_t}{N_0} = \int_{-\infty}^{\hat\beta} g_0(\beta)\,d\beta. \tag{17}$$

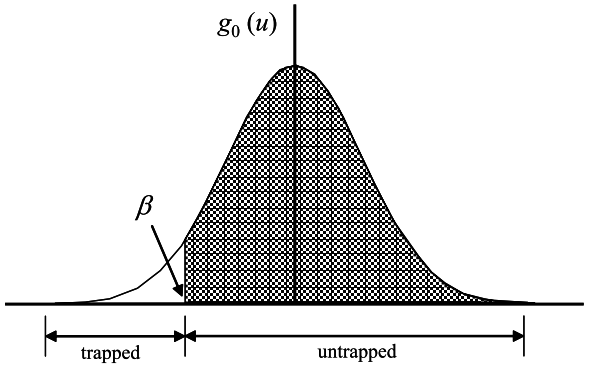

Fig. 4. Integration range for the kinetic term of untrapped particles.

Note that K_t is self-consistently obtained from test particle tracking, but the calculation of K_u requires some approximations like Eqs. (16) and (17). The validity of the approximations should be extensively investigated in the future especially for the high temperature regime, where the trapped particles are not small perturbations any more but have an active role in deforming the zero'th order distribution g_0.

3.3. Test particle mover and envelope solvers

The test particles are driven by the ponderomotive force of the counterpropagating lasers and the electrostatic field. The major difference of the test particle scheme from conventional PIC or the aPIC is that the electrostatic field is obtained not from the particle's charge but from the envelope-kinetic plasma Eq. (10). In other words, the test particles behave as electrons under a given field, but they do not generate any field. Therefore, Poisson's equation is not explicitly solved in the test particle scheme. The equation of motion for jth test particle is

$$\frac{\mathrm{d}u_j}{\mathrm{d}t} = -\frac{e}{m}E(z_j,t) - \frac{c^2}{2}\frac{\partial}{\partial z}\Re e[a_1^* a_2 e^{\mathrm{i}\phi}]_{\phi=\phi_j}, \tag{18}$$

where $\phi = -(k_1+k_2)z - (\omega_2-\omega_1)t$ and $\phi_j = -(k_1+k_2)z_j - (\omega_2-\omega_1)t$. The electric field is obtained by using $eE(z_j,t)/mc\omega_p = \Re eF(z_j)e^{\mathrm{i}\phi}$. The envelope F at the particle position z_j is interpolated from the grid values $F_{i-1/2}$, $F_{i+1/2}$, and $F_{i+3/2}$ for $i \leqslant z_j J/L < i+1$. Here, J and L are the total number of simulation grids and domain length, respectively. The envelopes on grid F_is are calculated by explicitly solving Eq. (10).

The laser envelope equation (5) is solved by the BSCT (backward-space-time-centered) scheme, which is one of the implicit methods, while the source term is treated explicitly.

3.4. Benchmarking

The test particle code was benchmarked against the aPIC code. The benchmarking was carried out for a wide variation of the laser and plasma parameters. The fluid three-wave calculations are also presented along with the kinetic simulations to show how the behavior of RBS can be modified by the particle trapping.

For all the simulations, a strong enough pump laser was used to cause the electron trapping. The normalized pump amplitude $a = eA/mc$ for that should be larger than 0.005 typically. We used $a_2 = 0.01$, 0.015, and 0.02, for various plasma parameters.

Fig. 5 is the comparison of the amplified seed profiles from the test particle simulation and corresponding aPIC simulation. The result from the fluid three-wave model is also presented. It is clear from the figure that the agreement between two kinetic simulations (test particle scheme and aPIC) is quite reasonable, while the deviation of the three-wave result is significant.

Instead of showing snapshots for all cases, it is much more efficient to show temporal evolution of the seed characteristics. The most important characteristics of the amplified seed are the peak amplitude and the longitudinal pulse duration. Figs. 6 and 7 show the evolution of the seed for various initial parameters. For most of the cases, the peak amplitudes from two different kinetic simulations agree well with each other, while the three-wave model overestimates the amplification level. The longitudinal pulse duration grows in the early stage of the amplification, which is called the linear regime. In this regime, the pump depletion is negligible, and the seed pulse grows with the linear growth rate. As the seed goes through the amplification, the pump begins to be significantly depleted and simultaneously the seed is compressed longitudinally, which is called the nonlinear regime. The evolution of the full-width-half-maximums (FWHMs) for $T_e = 10$ eV (Fig. 6) shows good agreement between the aPIC and test particle schemes both in the linear and nonlinear regimes. For relatively high temperature case of $T_e = 50$ eV in Fig. 7, the FWHMs in the linear regime are overestimated by the fluid model and underestimated by the test particle scheme. For high temperature plasmas, the electron trapping occurs even in the linear regime, which makes the rear part of the seed be more shrunken compared to the fluid results. In the test particle scheme, such effects are more or less enhanced over the aPIC case, possibly because the change in the zero'th order distribution g_0, which influences the integration equation (16), is not being considered. Though the minor discrepancy in the FWHM near the linear regime, more important

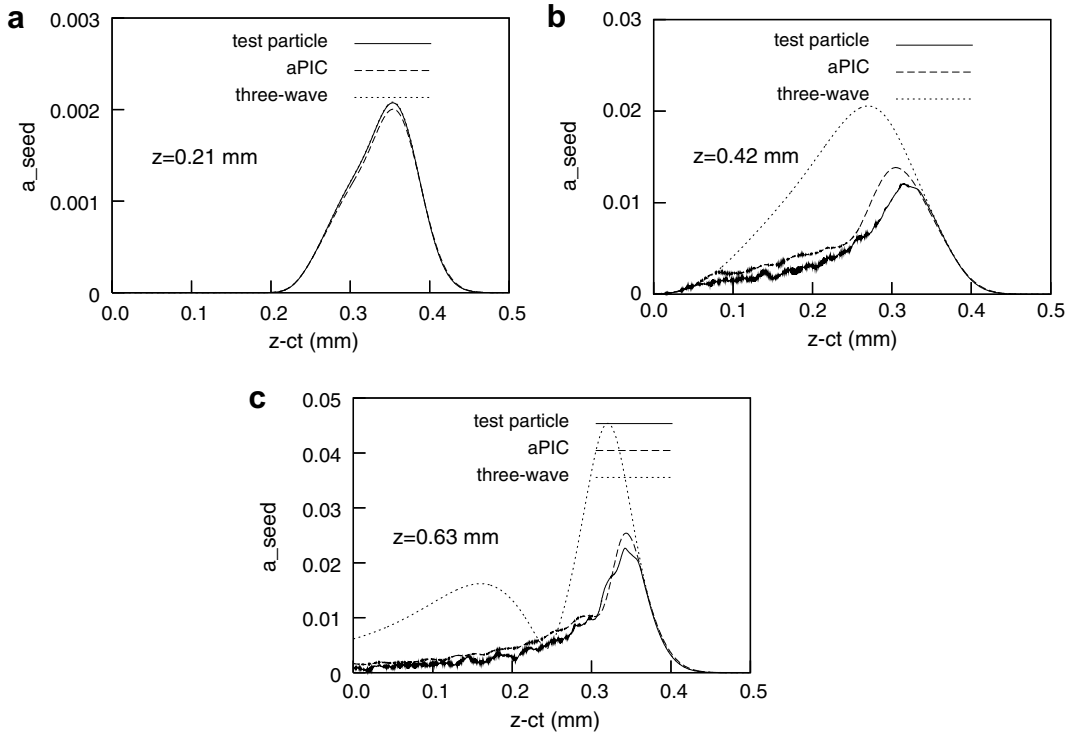

Fig. 5. Comparison of the seed profiles obtained from the test particle (solid), aPIC (dashed), and fluid three-wave (dotted) simulations. The pump laser amplitude was $a_2 = 0.015$. The initial seed amplitude is $a_1 = 0.000942$. The numbers of simulation particles in a single plasma wavelength are 4096 and 128 for the aPIC and the test particle simulations, respectively. The plasma density and temperature were $n_e = 1.05 \times 10^{19}\ \mathrm{cm}^{-3}$ and $T_e = 10$ eV, respectively.

results such as amplification level and the FWHM in the nonlinear regime exhibit reasonable agreement with the aPIC results even for the $T_e = 50$ eV case.

3.5. Computation speed of the test particle code

As mentioned previously, the computation speed-up of the test particle scheme is not only from the partial loading of the simulation particles, but also from the thermal-noise-free property of the envelope solvers. The thermal noise is intrinsic in plasmas, but it is numerically enhanced in the PIC codes (including the aPIC), since a single simulation particle corresponds to huge number of real particles. The numerically increased noise can distort severely the behavior of amplified seed. Fig. 8 shows the comparison of the seed snapshots from aPIC simulations with different numbers of simulation particles. The numbers of particles per mesh are $N_0 = 2560$ (solid), $N_0 = 1024$ (dashed), and $N_0 = 512$ (dotted), respectively, while all other parameters are the same. The pump laser amplitude is $a_2 = 0.02$ and $T_e = 50$ eV. As time advances, the seed profiles for $N_0 = 512$ and $N_0 = 1024$ cases deviate from the more refined simulation with $N_0 = 2560$. The numerically enhanced plasma noise includes the plasma wave component $\exp[-\mathrm{i}(k_1 + k_2)z - \mathrm{i}(\omega_2 - \omega_1)t]$, and the Raman growth depends on the initial level of such component. Hence the distortion of the pulse can be thought as the result of different Raman backscatter depending on the numerical conditions.

For the test particle simulation (double dotted) in Fig. 8d, the number density $N_0 = 512$ was used (so the number of test particles per mesh is just half of that). Though a very small number of particles was used, the test particle result is closer to the $N_0 = 4096$ aPIC even than $N_0 = 2560$ aPIC case. In the test particle scheme, the particle effects are counted via the kinetic term only in the trapped region, so there does not exist any numerical thermal noise in the seed front. This means that, as presented in Fig. 8d, the test particle simulation requires much smaller number of simulation particles to get as accurate result as the aPIC. The computation

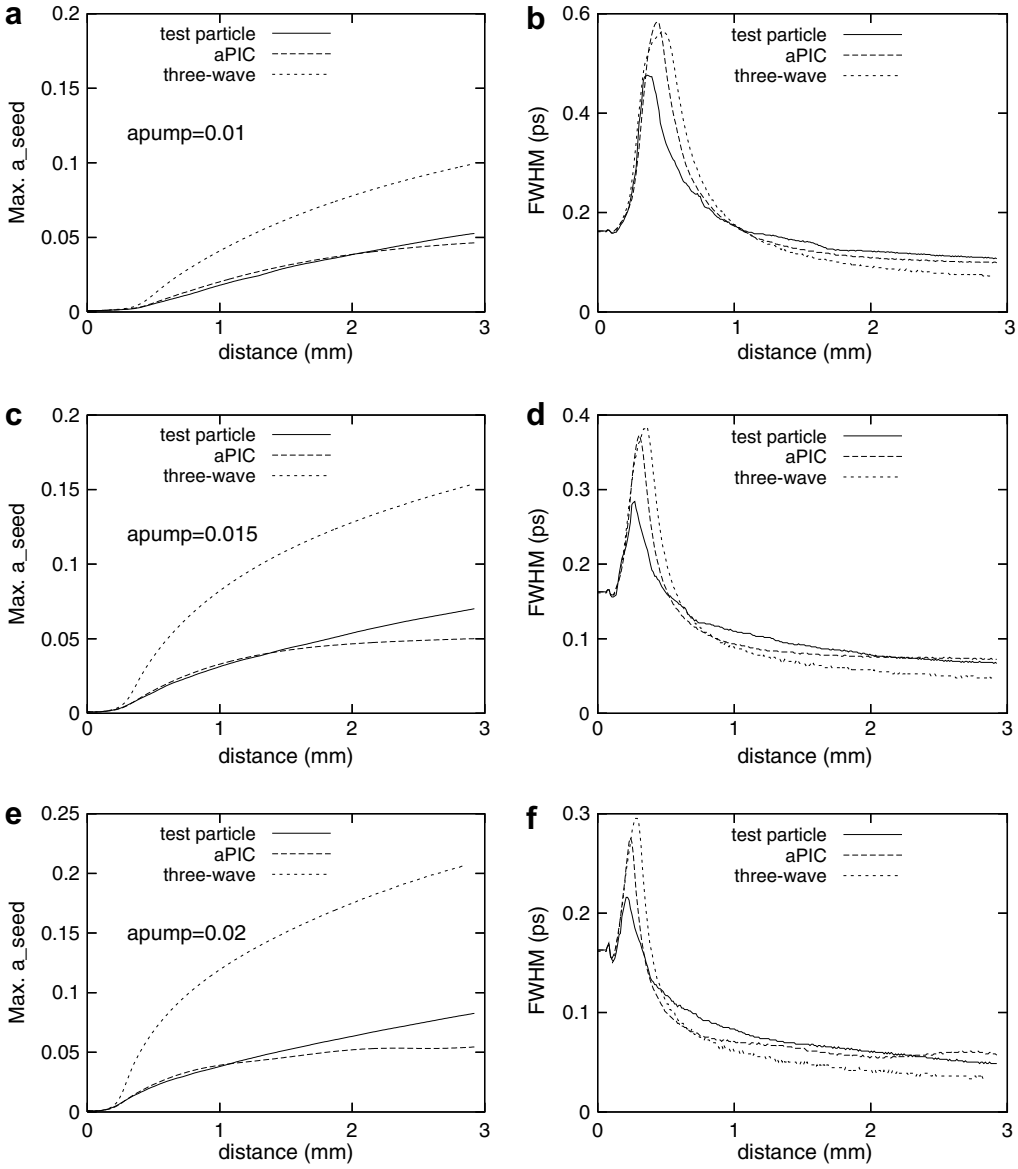

Fig. 6. Temporal evolutions of the peak amplitude and the FWHM of the seed for the pump laser (a,b) $a_2 = 0.01$, (c,d) $a_2 = 0.015$, and (e,f) $a_2 = 0.02$. The initial seed amplitude is the same as in Fig. 5. The numbers of simulation particles are 4096 and 256 for the aPIC and the test particle simulations, respectively. The plasma density and temperature were $n_e = 1.05 \times 10^{19}\ \mathrm{cm}^{-3}$ and $T_e = 10\ \mathrm{eV}$, respectively.

time for 1.8 mm propagation of the seed was 2200 s, while it took more than 44000 second, which is a speed-gain by a factor of 20.

4. Summary

It has been found that Raman backscatter and the Raman backward laser amplification are significantly influenced by the electron kinetic effects [3,5,4]. The amplification system has been commonly modeled by the three-wave fluid equations. In the kinetic regime, however, the fluid-based three-wave model cannot reproduce the results from kinetic codes such as PIC or aPIC. In this paper, a new test particle method was sug-

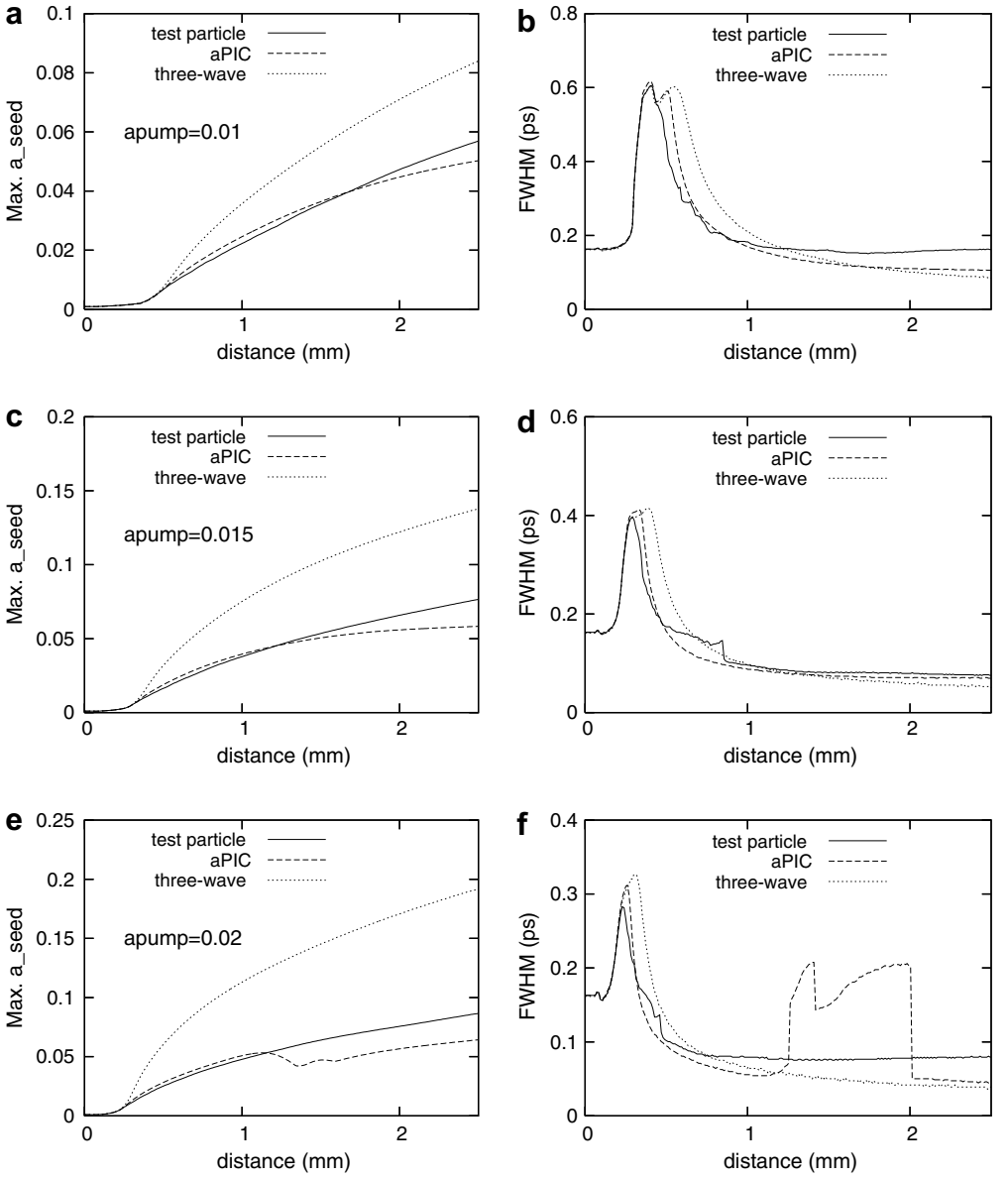

Fig. 7. Temporal evolutions of the peak amplitude and the FWHM of the seed for the pump laser (a,b) $a_2 = 0.01$, (c,d) $a_2 = 0.015$, and (e,f) $a_2 = 0.02$. The initial seed amplitude is the same as in Fig. 5. The numbers of simulation particles are 4096 and 512 for the aPIC and the test particle simulations, respectively. The plasma density and temperature were $n_e = 1.05 \times 10^{19}\ \mathrm{cm}^{-3}$ and $T_e = 50\ \mathrm{eV}$, respectively.

gested for the self-consistent incorporation of the kinetic effects into the envelope three-wave model. In this new scheme, the laser envelopes are solved by the same equations used in the conventional three-wave model. For the calculation of the plasma wave envelope, however, the envelope-kinetic plasma equation is used instead of the pure envelope equation. The most important feature of the envelope-kinetic plasma equation is the kinetic term, which is an ensemble average of particles' velocity squares weighted by their ponderomotive phases. Then, the core of the new scheme is using test particles to calculate the kinetic term self-consistently. The test particles follow the normal equation of motion, while they do not generate any field. The benchmarkings of the test particle scheme against the aPIC simulations show quite a reasonable agreement in a wide range of laser and plasma parameters. The computation speed gain of the new scheme from the aPIC is at least a factor of two, as it loads just negative half in the full velocity distribution, which are relevant to the

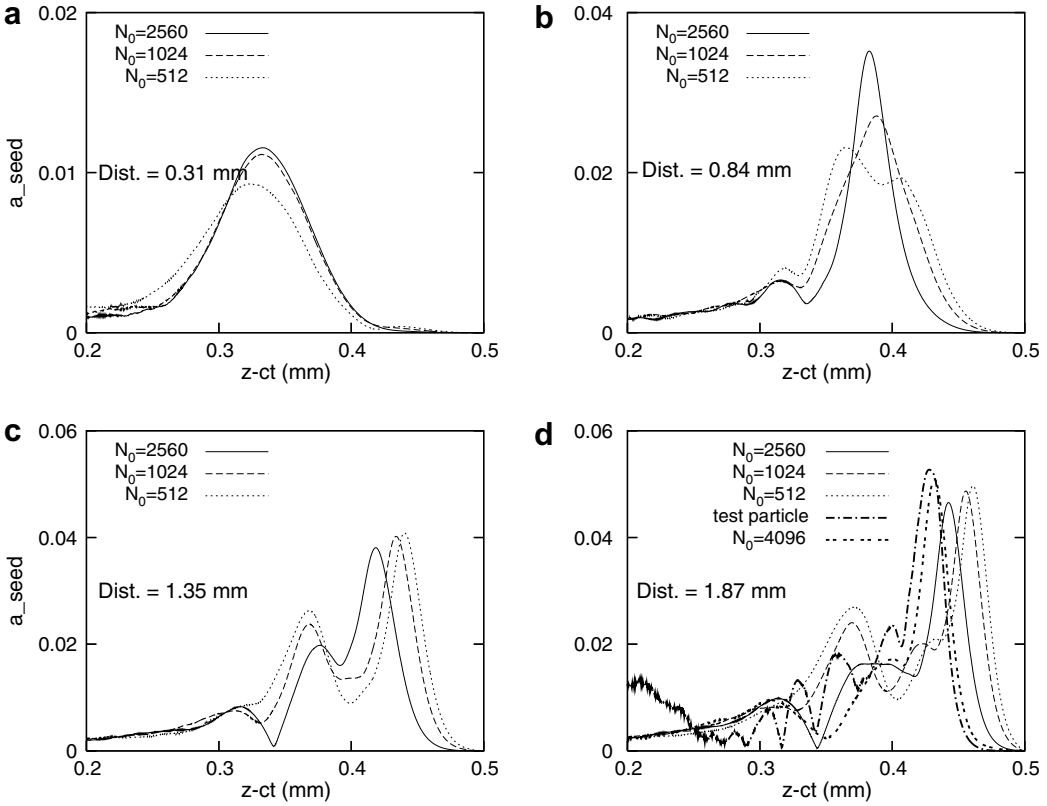

Fig. 8. Seed snapshots for different numbers of simulation particles, obtained from aPIC simulations. N_0 represents the number of particles per mesh. The profiles were measured after the seed propagation (a) 0.31 mm, (b) 0.84 mm, (c) 1.35 mm, and (d) 1.87 mm. The plasma density was $n_e = 1.05 \times 10^{19}$ cm^{-3}, the temperature 50 eV, and the pump laser amplitude was $a_2 = 0.02$. The test particle result and $N_0 = 4096$ cases are plotted together in (d) for the comparison.

trapping. However, because the test particle scheme is free from the numerically enhanced thermal noise, it is possible to get as accurate results as the aPIC simulations with much smaller number of test particles. Thus the speed gain can be much larger, sometimes reaching a factor of 20 depending on parameters. In this paper, the low temperature regime where the Landau damping is negligible was considered. Since the kinetic term generally includes the linear and nonlinear Landau damping, the test particle scheme can be made valid in the high temperature regime also. However, some modifications in Eqs. (16) and (17)are required, since the linear Landau damping would change the zero'th order distribution function g_0 quickly. The refined modeling for that remains as future issues.

Acknowledgement

This work was financially supported by the Creative Research Initiatives program/KOSEF of Korea Ministry of Science and Technology.

References

[1] S.V. Bulanov, F. Pegoraro, A.M. Pukhov, A.S. Sakharov, Phys. Rev. Lett. 78 (1997) 4205.
[2] S.V. Bulanov, N. Naumova, F. Pegoraro, J. Sakai, Phys. Rev. E 58 (1998) R5257.
[3] M.S. Hur, R.R. Lindberg, A.E. Charman, J.S. Wurtele, H. Suk, Phys. Rev. Lett. 95 (2005) 115003.
[4] M.S. Hur, I. Hwang, H. Suk, J. Korean Phys. Soc. 47 (2005) 625.
[5] M.S. Hur, S.H. Yoo, H. Suk, Phys. Plasmas 14 (2007) 033104.

[6] H.X. Vu, D.F. DuBois, B. Bezzerides, Phys. Rev. Lett. 86 (2001) 4306.
[7] H.X. Vu, D.F. DuBois, B. Bezzerides, Phys. Plasmas 9 (2002) 1745.
[8] J.M. Dawson, Phys. Rev. 113 (1959) 383.
[9] D.S. Clark, N.J. Fisch, Phys. Plasmas 10 (2003) 4848.
[10] P. Mardahl, H.J. Lee, G. Penn, J.S. Wurtele, N.J. Fisch, Phys. Lett. A 296 (2002) 109.
[11] A. Pukhov, J. Meyer-ter-Vehn, Appl. Phys. B 74 (2002) 355.
[12] A. Zhidkov, J. Koga, T. Hosokai, K. Kinoshita, M. Uesaka, Phys. Plasmas 11 (2004) 5379.
[13] H.X. Vu, B. Bezzerides, D.F. DuBois, J. Comp. Phys. 156 (1999) 12.
[14] C. Huang, V.K. Decyk, C. Ren, M. Zhou, W. Lu, W.B. Mori, J.H. Cooley, T.M. Antonsen Jr., T. Katsouleas, J. Comp. Phys. 217 (2006) 658.
[15] D.F. Gordon, W.B. Mori, T.M. Antonsen Jr., IEEE Trans. Plasma Sci. 28 (2000) 1135.
[16] M.S. Hur, G. Penn, J.S. Wurtele, R.R. Lindberg, Phys. Plasmas 11 (2004) 5204.
[17] V.M. Malkin, G. Shvets, N.J. Fisch, Phys. Rev. Lett. 82 (1999) 4448;
V.M. Malkin, G. Shvets, N.J. Fisch, Phys. Plasmas 7 (2000) 2232.
[18] G. Shvets, J.S. Wurtele, B.A. Shadwick, Phys. Plasmas 4 (1997) 1872.
[19] G. Shvets, N.J. Fisch, A. Pukhov, J. Meyer-ter-Vehn, Phys. Rev. Lett. 81 (1998) 4879.